Low-loss singlemode PECVD silicon nitride photonic wire waveguides for 532-900 nm wavelength window fabricated within a CMOS pilot line

A.Z. Subramanian, A. Dhakal, F. Peyskens, S. Selvaraja*, *Member,* IEEE and R. Baets, *Fellow*, IEEE
Photonics Research Group, Ghent University-IMEC, Ghent 9000, Belgium
Centre for Nano- and Biophotonics, Ghent University, Ghent 9000, Belgium
*Currently with IMEC, Kapeldreef, Leuven 3001, Belgium

P. Neutens, R. Jansen, T. Claes, X. Rottenberg, P. Helin, B. Du Bois, K. Leyssens, S. Severi, P. Deshpande and P. Van Dorpe
IMEC, Kapeldreef, Leuven 3001, Belgium

Abstract: PECVD silicon nitride photonic wire waveguides have been fabricated in a CMOS pilot line. Both clad and unclad single mode wire waveguides were measured at λ=532 nm, 780 nm and 900 nm respectively. The dependence of loss on wire width, wavelength and cladding is discussed in detail. Cladded multimode and singlemode waveguides show a loss well below 1 dB/cm in the 532-900 nm wavelength range. For singlemode unclad waveguides losses < 1 dB/cm was achieved at λ=900 nm whereas losses were measured in the range of 1-3 dB/cm for λ=780 and 532 nm respectively.

Index Terms: Waveguides, Waveguide devices, Fabrication and characterization, Photonic materials, Gratings.

1. Introduction

Silicon photonics has evolved to become a real-world technology. The combination of high-index-contrast (HIC) and compatibility with complementary-metal-oxide-semiconductor (CMOS) processing has helped in low-cost and high volume production of high-quality photonic components and circuits. The major driving force behind silicon photonics remains the integration of photonic and electronics components on a common silicon-based platform mainly related to on-chip interconnects and telecom applications. In recent years, there has been a tremendous surge of interest towards integration of photonic devices with different functionalities on a chip for biological sensing and detection [1-2]. Examples include lab-on-a-chip based systems for evanescent field based sensing [3], fluorescence [4] and Raman spectroscopy [5]. For such applications, the visible and very-near-infrared (VNIR) (500-950 nm) wavelength window is of particular interest due to minimal photo damage to living cells, negligible water absorption, low fluorescence, and the availability of low-cost sources and sensitive silicon-based detectors.

However, for all its technological development silicon remains transparent only for wavelengths > 1.1 μm thereby making it unsuitable for most of the bio-related applications that require shorter wavelengths in the visible-VNIR range for optimum performance. Silicon nitride (Si_3N_4) is a well-known dielectric material that is transparent in the visible-NIR and beyond, compatible with CMOS-based processes for low-cost mass fabrication, possesses relatively high refractive index (n~2.0) for tighter confinement, does not suffer from two-photon absorption, and has lower temperature sensitivity than silicon. Predominantly, Si_3N_4 is deposited using low-pressure chemical vapour deposition (LPCVD) or plasma-enhanced chemical vapour deposition (PECVD) technique. Of the two, LPCVD is often preferred as it provides an excellent control over the homogeneity of material index and thickness. However, it remains a high-temperature process (>700^{o}C) and it induces high stress, particularly in the thicker films (>300 nm) making it unsuitable for many integrated optical devices. On the other hand, PECVD is a low-temperature process (200-400^{o}C) and enables stress-free thicker film deposition, making it a better alternative for many photonic-based applications. However, the film homogeneity is poorer than in the case of LPCVD films. Therefore, a well-optimized process for low-loss Si_3N_4 waveguides using PECVD provides a very attractive route towards high-volume fabrication of integrated photonic devices.

So far, low-loss Si_3N_4 waveguides in the visible-VNIR have been fabricated mostly by LPCVD [6-8]. Low-loss (< 1 dB/cm) in these waveguides was achieved by restricting the etch-depth to low values (5 nm) [6] or by making wide (> 10 μm) multimode waveguides [7] in combination with complete cladding of the waveguide by SiO_2. Gorin et al. demonstrated low-loss (<0.5 dB/cm) high-index PECVD slab waveguides in the 470 nm-633 nm wavelength range [9]. This was achieved by optimizing precursor gas ratio, low-frequency PECVD that reduced the absorption losses and rapid thermal annealing of the waveguides. Recently, singlemode photonic wire (cladded) with low waveguide (<0.7 dB/cm) and bend (<0.05 dB/90^o) loss fabricated within a CMOS pilot-line was demonstrated for the first time at 660 nm using PECVD technology [10]. However, the dependence of waveguide loss on different parameters such as wavelength (within the visible-VNIR range), waveguide width and cladding is yet to be reported. In this work, we compare PECVD nitride photonic wires fabricated in a CMOS pilot-line for different wavelengths (532, 780 and 900 nm), singlemode widths, and cladding conditions respectively. Waveguide loss of < 1 dB/cm was achieved for cladded waveguides at 532 nm and 900 nm wavelength.

2. Waveguide Design and Simulations

For Si_3N_4 waveguide characterization a test mask was designed comprising of straight and spiral waveguides of different lengths (1, 2, 4 and 8 cm) and different widths with grating couplers (GCs) at each end for input and output coupling of light. The Fimmwave mode solver was used for design and simulation. A cross-section of 180-220 nm height and width in the range of 300-1000 nm was used for the core of the Si_3N_4 waveguide. It was found that the minimum oxide thickness to avoid any significant leakage into the substrate was 1.5 µm; therefore in the simulations the oxide thickness was taken as 2.0 µm. The above geometry of Si_3N_4 waveguide ensured singlemode operation in the complete visible-VNIR range. The grating couplers (GCs) were designed using CAMFR, an eigenmode expansion tool [11-12]. The GCs were designed for TE polarization and the corresponding period, linewidth and etch-depth was calculated for different wavelengths (532, 780 and 900 nm) as described in our previous work on the GCs for NIR wavelength [13].

Fig. 1 shows the dispersion results for the Si_3N_4 waveguides at different wavelengths for different widths for both cladded and uncladded waveguides. The cladded waveguides received a 2 µm thick PECVD SiO_2-top coating. The refractive index of Si_3N_4 was taken as 1.93 (at 532 nm) and 1.89 (at 780 nm and 900 nm) and, 1.46 as the index of SiO_2 respectively. The refractive indices were determined by ellipsometry on the deposited Si_3N_4 and SiO_2 thin films (to be discussed in the next section). The Si_3N_4 height was taken as 180 nm for λ=532 nm and, 220 nm for λ=780 nm and λ=900 nm respectively. Based on the above parameters, the singlemode width at 532 nm wavelength was determined to be ~380 nm for the cladded and ~530 nm for the unclad waveguides. At 780 nm, singlemode width was 900 nm for the unclad waveguide and ~630 nm for the cladded waveguide, and finally the corresponding singlemode width at 900 nm wavelength was ~1100 nm for the unclad and ~770 nm for the cladded waveguide respectively. It should be noted that an unclad waveguide reaches cutoff for widths ≤ 500 nm at 900 nm wavelength as depicted in fig. 1(c).

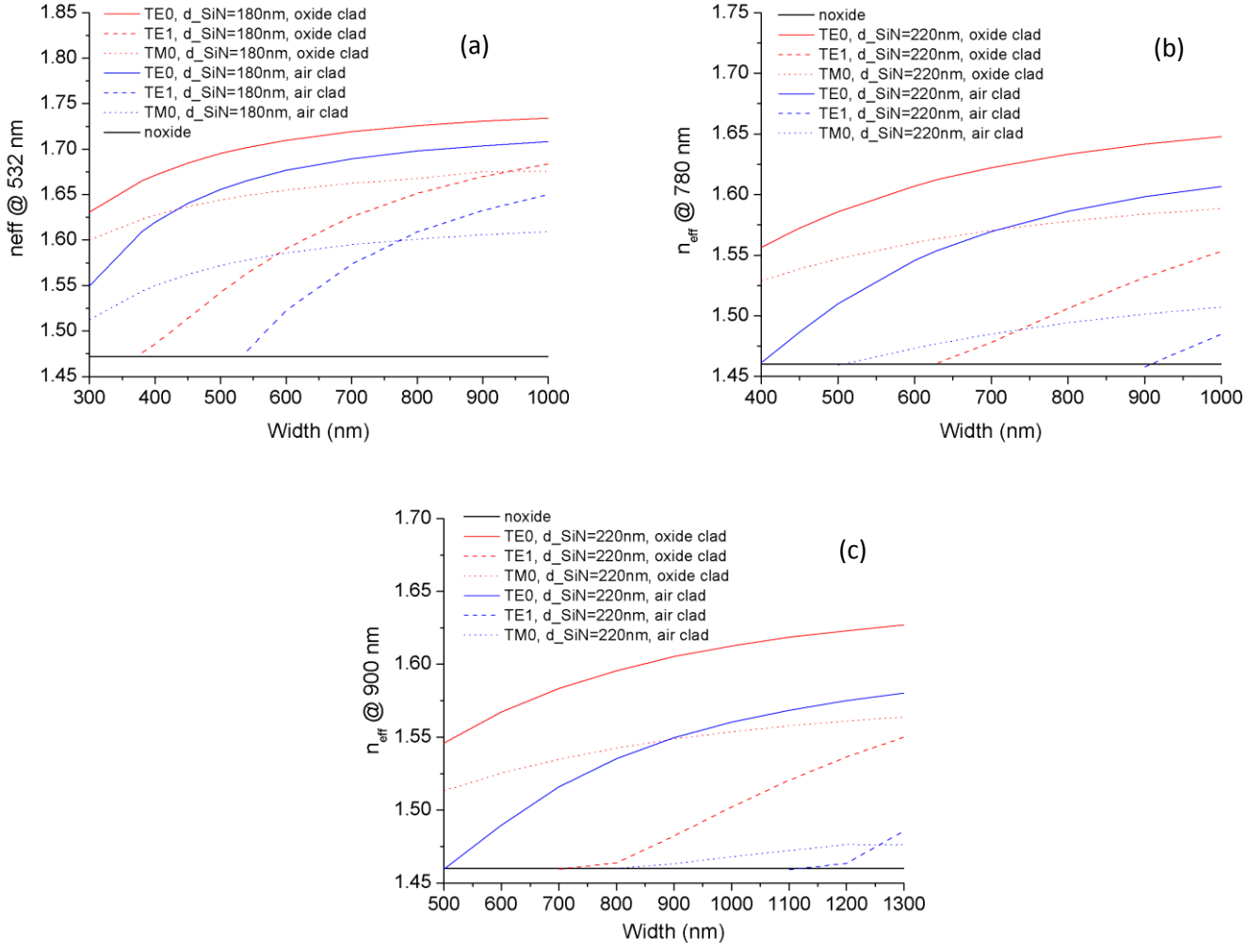

Fig. 1. Dispersion diagram for Si_3N_4 waveguides for different widths and wavelengths (a) 532 nm, (b) 780 nm and (c) 900 nm.

3. Waveguide Fabrication and Characterization

To build a photonic circuit in Si_3N_4, we start with a 200 mm bare silicon wafer. After cleaning the wafer, 2-2.4 µm of silicon dioxide (SiO_2) was deposited using a high-density plasma (HDP) CVD process. On top of the isolating oxide, Si_3N_4 was

deposited using PECVD on different wafers. Two thicknesses of Si_3N_4 were chosen, 180 nm Si_3N_4 stack for 532 nm wavelength and 220 nm Si_3N_4 stack for 780 and 900 nm wavelength operation respectively. PECVD Si_3N_4 was deposited using SiH_4, N_2 and NH_3 at 400^oC, which ensured CMOS back-end compatibility. The precursor gas-ratio was chosen as to minimize loss, following the results of ref. [8]. After the layer deposition, waveguides and grating couplers were patterned by using 193 nm optical lithography. This was followed by the inductive coupled plasma-reactive ion-etch process, using fluorine-based etch chemistry. The waveguides were completely etched to form strip waveguides with different widths (300-1000 nm) and the GCs were partially etched (70-140 nm) by tuning the etch duration. The optimum value for the underlying oxide thickness and etch-depth for GCs was based on a previous study on the optimization of GC at 900 nm wavelength [13]. Photoresist was used as an etch-mask for both etch processes. After dry etching, the wafers were cleaned by using oxygen plasma and a wet chemical process. Since Si_3N_4 does not possess any absorption band in the visible-VNIR wavelength range, therefore no annealing or thermal treatment was applied to the nitride samples.

The refractive index and thickness of the film were determined by ellipsometry. The film quality in terms of roughness was determined using atomic force microscopy (AFM) on both the SiO_2 and Si_3N_4 films. Finally, the propagation loss in the wire waveguide was measured at different wavelengths by cut-back method using spiral waveguides with different lengths and bend radius. The measurements were done by coupling light from a laser source using a singlemode fibre through an input GC into the Si_3N_4 waveguide. Another similar fibre is positioned above an output GC to collect the light into a power meter. The position of the fibre was optimized for the maximum transmission. These measurements were performed for TE polarisation using different laser sources (532, 780 and 900 nm).

4. Experimental Results and Discussion

4.1. Optical characterization of the Si_3N_4 thin film

The ellipsometry measurements were performed on the as-deposited Si_3N_4 thin films. A fit to the experimental values using Cauchy dispersion model yielded the best results for the index and thickness. The value of the thickness as determined by the Cauchy model compared well with the measured thickness value using stylus profilometer. Fig. 2 shows the refractive index vs. wavelength for the fully optimized Si_3N_4 thin films. A refractive index of ~1.89 was measured for the Si_3N_4 at 780 nm. A standard 9-point thickness measurement was performed on one of the test wafers from the lot. An average thickness of 178.9 nm was obtained with a standard deviation of 4.6 nm for a targeted value of 180 nm. The minimum and maximum thicknesses were 174.2 and 186.2 nm respectively.

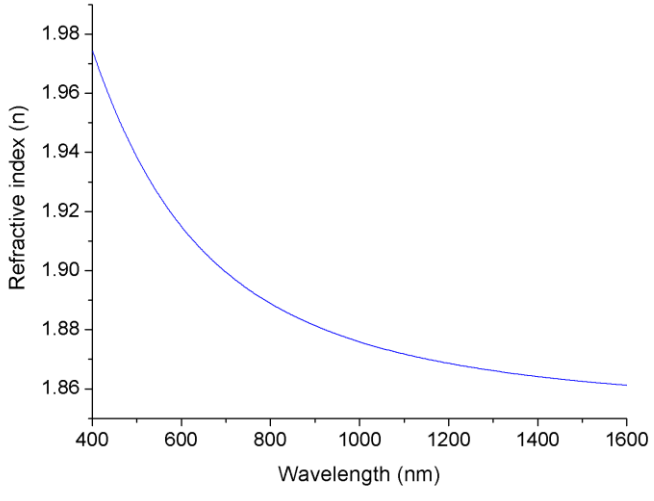

Fig. 2. Refractive index of as-deposited Si_3N_4 thin film determined by ellipsometry

The film quality in terms of roughness for both the SiO_2 and Si_3N_4 thin films was determined using AFM. In order to have a low scattering loss the deposited thin film (both oxide and nitride) should be as smooth as possible. Any roughness present on the oxide layer is transferred to the nitride layer deposited later on top that eventually leads to light scattering out of the waveguide. The 3D representation of the root mean square (r.m.s.) roughness value of the films (2 µm HDP SiO_2 and 100 nm PECVD Si_3N_4 on top of 2 µm HDP SiO_2) measured using AFM is shown in Fig. 3. The measurements were done with the help of an AFM probe by scanning the top surface of both the SiO_2 and Si_3N_4 films over an area of 2 µm x 2 µm. The r.m.s roughness value for the 2 µm HDP SiO_2 film was measured to be extremely low at 0.13 nm (Fig. 3(a)) and the 100 nm Si_3N_4 film deposited on top of oxide also exhibited a very low r.m.s. roughness value of 0.28 nm (Fig. 3(b)).

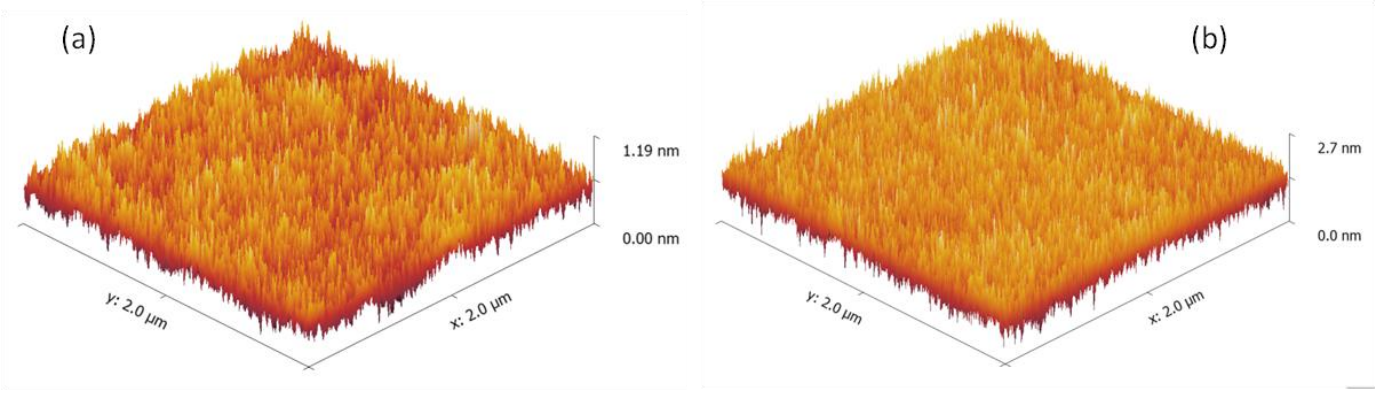

Fig. 3. RMS roughness value measured by AFM of (a) SiO_2 and (b) as-deposited Si_3N_4 thin film

4.2. Optical Characterization of the Si_3N_4 wire waveguide

The Si_3N_4 strip waveguides were inspected under scanning electron microscope (SEM) for measuring the waveguide dimension and analyzing the etch quality of the waveguides. On the test wafers for measurements at 532 nm, the bottom cladding was 2 µm HDP silicon dioxide, optimized to give the highest GC efficiency. The thickness of the nitride stack was fixed at 180 nm whereas the waveguide width was varied from 300 nm to 1000 nm. For cladded waveguides, another layer of 2 µm SiO_2 was deposited on top of the waveguides. For the 780 and 900 nm wavelengths, the bottom oxide cladding was 2.4 µm HDP SiO_2. The thickness of Si_3N_4 was fixed at 220 nm and width was varied between 450 and 800 nm. Fig.4 shows the SEM pictures of the cross-section of one such fabricated waveguide corresponding to the 220 nm Si_3N_4 waveguide and one of the GCs. The cross-section of the waveguide and GC were made using focused ion beam (FIB) and were analysed using SEM. The relatively low-index-contrast between Si_3N_4 and SiO_2 (as compared to SiO_2 and silicon) leads to low contrast SEM images due to which there is no marked distinction between Si_3N_4 and SiO_2 layers in Fig 4. In order to avoid charging effects, a thin layer of gold was deposited prior to FIB/SEM measurement. The nominal width of the waveguide (on the mask) was designed to be 500 nm and the measured width on the chip was 485 ± 25 nm. The Si_3N_4 thickness was measured to be 230 ± 15 nm for a targeted value of 220 nm. This is depicted in Fig. 4(a). It is also evident from Fig. 4(a) that there is a slight over-etching of the nitride leading to an etching of around 20-40 nm of the underlying oxide as well. Fig. 4(b) shows the entire cross-section of the waveguide along with the underlying oxide layer. The targeted oxide thickness was 2.4 µm and the measured thickness is found to be the same. However, across the wafer the oxide thickness was found to vary by over 5%. Lastly, Fig. 4(c) shows the cross-section of the GCs. The intended period and etch depth of the GC was 630 nm and 140 nm respectively. The measured period and etch depth was found to be 620 nm and 135 nm which is in reasonable agreement with the nominal value.

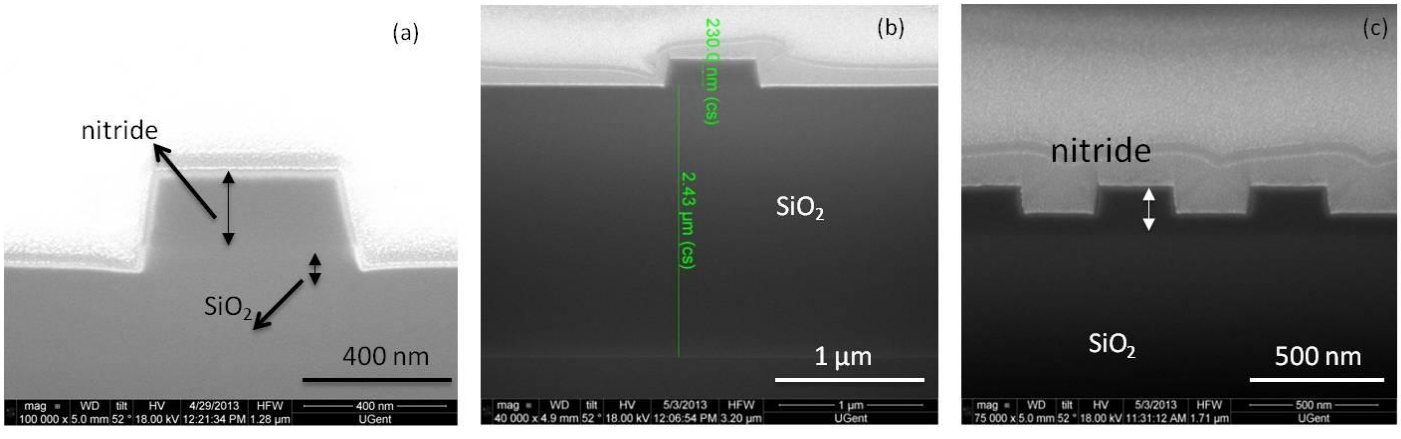

Fig. 4. SEM pictures of Si_3N_4 cross-section prepared by FIB (a) Si_3N_4 waveguide, (b) complete cross-section including underlying SiO_2 and (c) GC with 630 nm period and 140 nm etch depth

Two types of GCs were designed linear GC and curved GC but for all the results discussed in this paper, only the LGC is considered. In case of LGC for 780 and 900 nm, two GCs at either end of the waveguide were defined on a 8 μm wide waveguide which was adiabatically tapered down to the desired wire width. Whereas for 532 nm, a 5 µm wide waveguide was used together with a taper of 125 µm length. The period of the GC was fixed for different wavelengths of operation whereas the etch depths (70, 120, 140 nm) and fill factor (0.45, 0.5, 0.55, 0.6) were varied. For 532 nm wavelength operation, the period of the GC was fixed at 365 nm, for 780 nm wavelength, the period was fixed at 530 nm and finally for 900 nm wavelength, the period was fixed at 630 nm respectively. Typical efficiency of these GCs were around ~7 dB/coupler that is comparable to standard GCs used in silicon photonics. However, being a deposited material it is very much possible to improve the efficiency of the coupler to <3 dB/coupler through the use of distributed Bragg reflector [13-14] or as recently shown by using metallic reflectors underneath the film [15-16]. The cladded samples due to the reduced grating index

showed an improvement in the coupling efficiency to ~6 dB/coupler with a slight blue shift in the peak wavelength.

The variation in the waveguide loss for the different widths of the unclad Si_3N_4 wire at 532 nm, 780 nm and 900 nm wavelengths is shown in Fig. 5. The waveguides exhibited < 1 dB/cm for wider widths (>700 nm) for both 532 nm and 900 nm wavelengths. For the widths in the range of 500 nm-700 nm, the wires showed losses in the range of 1-2 dB/cm for all the three wavelengths whereas for the widths < 500 nm relatively higher waveguide loss was measured. At 532 nm wavelength, waveguide widths in the range of 300-1000 nm were measured and the best loss value was achieved for the waveguides wider than 800 nm at 0.65 dB/cm. At 780 nm wavelength, four different widths (450, 500, 600 and 700 nm) were measured and the best loss value measured was 1.33 dB/cm for 700 nm wide waveguide. Finally at 900 nm wavelength, four widths (500, 600, 700 and 800 nm) were measured and the best loss values were exhibited by 800 nm wide waveguides at 0.62 dB/cm. The 500 nm wide waveguide showed much higher transmission loss. This is because around 500 nm the mode is close to cut-off as shown in Fig. 1 and the cutback method could not be trusted anymore consequently the loss values at 500 nm wide waveguide at λ=900 nm is not shown in Fig. 5

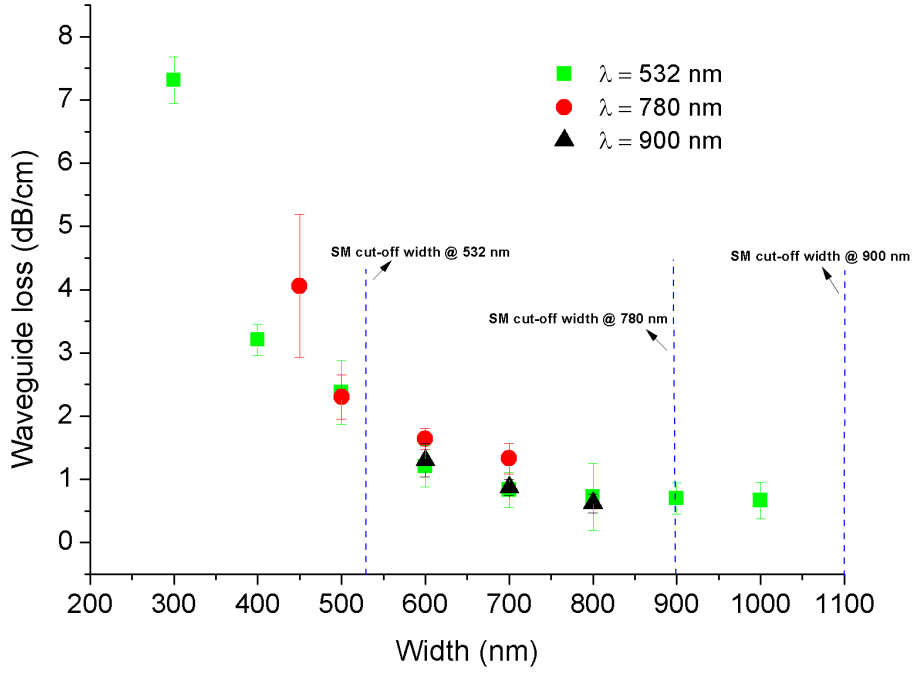

Fig. 5. Waveguide loss variation for the different widths of unclad Si_3N_4 waveguide at 532, 780 and 900 nm.

The waveguide loss variation for different widths and different wavelengths for cladded samples is shown in Fig. 6. At 532 nm wavelength, the waveguides showed a loss of < 1 dB/cm for 400 nm wide wire (singlemode) and the losses gradually dropped to beyond the measuring accuracy of the set-up (< 0.1 dB/cm) for wider waveguides. For the widths < 400 nm, the waveguide loss was < 2 dB/cm. At 900 nm wavelength, loss was < 1 dB/cm for the entire singlemode regime of 500-800 nm wide waveguides. The best loss measured was 0.3 dB/cm for 800 nm wide waveguide. Due to the presence of upper cladding, the 500 nm wide waveguide also exhibited low loss unlike unclad waveguide where the waveguide went into cut-off (Fig. 1).

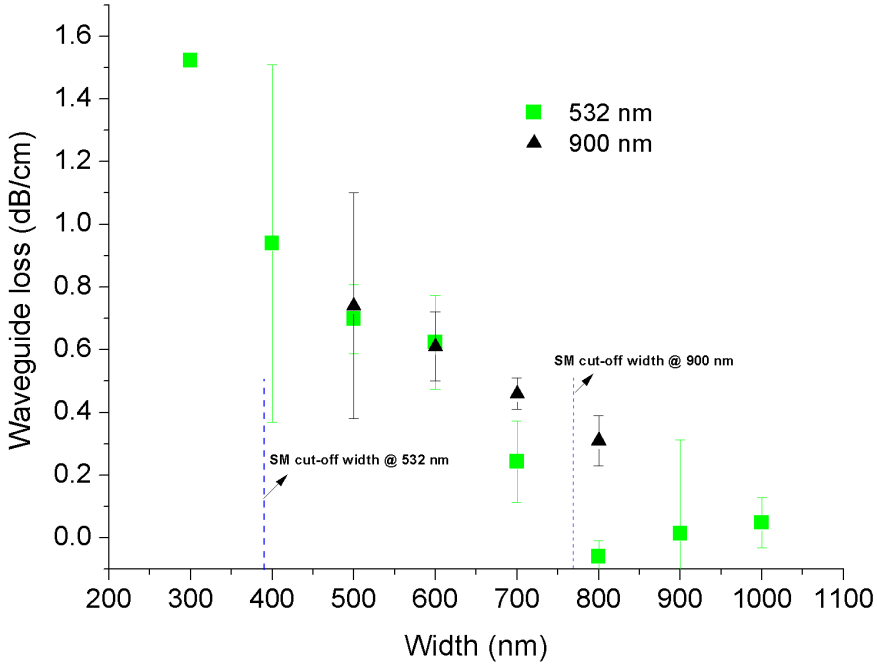

Fig. 6. Waveguide loss variation for the different widths of clad Si_3N_4 waveguide at (a) 532 nm and (b) 900 nm)

The loss behaviour observed for the Si_3N_4 wire waveguides- the reduction in the loss for the clad samples and for the wider waveguides, together indicate the presence of sidewall roughness. As is clear from the AFM results in Fig. 3 that shows negligible roughness on the deposited film itself so etching is believed to have caused some roughness on the sidewalls. The loss pattern observed at 900 nm wavelength is mainly attributed to the presence of sidewall roughness that leads to excess scattering thereby increasing the loss. At 780 nm wavelength, Rayleigh scattering is stronger than at 900 nm (~ $1/\lambda^4$) and in the presence of sidewall roughness, this scattering becomes more prominent leading to higher loss than at 900 nm wavelength. At narrow widths such as 450 nm (at λ=780 nm) and 500 nm (at λ=900 nm), waveguides are closer to cut-off (see Fig. 1) which leads to an increased leakage loss into the substrate and together with the sidewall roughness contributes to the overall waveguide loss. This puts an upper limit on the minimum width of the waveguide that can be used for practical applications. At 532 nm wavelength, the wider waveguides (>600 nm) show losses <1 dB/cm since the waveguides are multimode which increases the confinement of the mode resulting in less influence of the sidewalls on the waveguide loss. But in the singlemode regime (<600 nm) the effect of the sidewalls and Rayleigh scattering increases significantly which causes the waveguide loss to increase exponentially.

As already seen in Fig. 6 that the use of cladding has significant effect on the loss values and losses < 1 dB/cm is achieved in 532-900 nm wavelength range. But applications such as evanescent field based sensors demand unclad singlemode waveguides with low-loss values. In order to have similar losses (< 1 dB/cm for the 532-900 nm wavelength range) in unclad Si_3N_4 wire waveguides, slight improvement in the etching process is envisaged to reduce the sidewall roughness. In addition, wider waveguides tend to have lower losses (Fig. 5) which also makes fabrication tolerances much less stringent and less prone to fabrication imperfections. For example, the singlemode widths for the wavelengths 780 and 900 nm, as shown in Fig. 1, are 900 nm and 1100 nm respectively. Such wide waveguides are expected to yield lower loss even when unclad and are favorable in terms of fabrication tolerances as well.

Finally, to test the uniformity of the fabrication process the loss was measured on different dies across a wafer. Fig. 7(a) shows the regions from where the dies were selected whereas Fig. 7(b) shows the actual loss measured from these dies at 900 nm wavelength. Each data point on the Fig. 7(b) represents an average over three different waveguides from each die. The samples used were unclad and had a wire width of 800 nm. The result shows a reasonable uniformity in the performance of the waveguide across the wafer. The dies (4, 5, 6, and 7) towards the centre of the wafer showed lower loss (<0.8 dB/cm) whereas the dies (10-12) towards the edge showed slightly higher loss (~ 1 dB/cm). This is because close to the edge of the wafer the fabrication non-uniformity is the greatest resulting in imperfections and higher losses. The result for die #3 is not shown in Fig. 7 as it was not possible to measure the waveguide due to unwanted debris sticking to the waveguide surface that could not be removed. It is worth mentioning here that the wafer measured was not tiled and it is widely accepted that wafer-tiling leads to an uniform exposure and reaction of the material to the etching process and consequently to an uniformity in the device's performance. The loss variation across the wafer along with the uniformity in the thickness of the thin film points towards a good stable process for the fabrication of the waveguides.

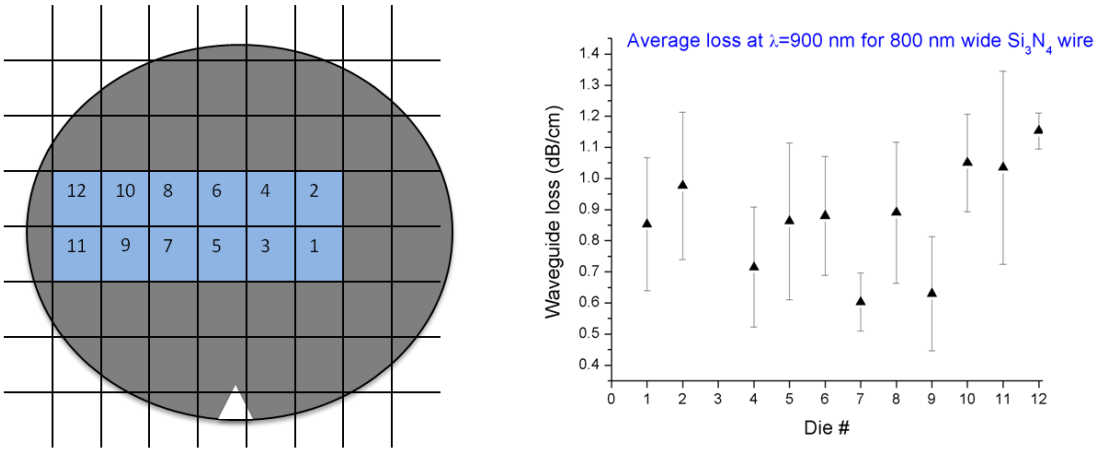

Fig. 7. Waveguide loss variation across wafer for different dies of 800 nm wide unclad Si_3N_4 waveguide at 900 wavelength. The die location is shown in (a), whereas the corresponding waveguide loss in (b)

5. Conclusions

We have demonstrated low-loss singlemode PECVD photonic wire waveguides fabricated in a CMOS pilot line for visible-VNIR wavelength applications. The PECVD nitride thin film was measured to have a refractive index of 1.89 at 780 nm and it showed a very smooth surface (r.m.s. roughness ~0.28 nm). The waveguide losses were measured using cutback method and were performed at 532, 780 and 900 nm wavelengths respectively, for Si_3N_4 wires with a height in the range of 100-220 nm and widths in the range of 450-800 nm. Both unclad and SiO_2 cladded waveguides were measured and the losses were compared. The Si_3N_4 wire waveguide losses exhibited a large dependence on the width and upper cladding condition. Cladded singlemode Si_3N_4 wires exhibited low-loss (<1 dB/cm) in the 532-900 nm wavelength regime whereas the unclad singlemode wire waveguides exhibited losses <1 dB/cm only at 900 nm and higher loss of 2.3 dB/cm (at 532 nm) and 1.33 dB/cm (at 780 nm) respectively. A good uniformity along the wafer was measured in terms of index, thickness and waveguide loss indicating stable process for reproducible results.

Acknowledgements

The authors (AZS, AD, FP and RB) acknowledge support from the ERC-InSpectra Advanced Grant. FP also acknowledges support from Bijzonder Onderzoekfonds (BOF) of Ghent University. PN acknowledges funding from Fonds Wetenschappelijk Onderzoek Vlaanderen (FWO)

References

[1] X. Fan and I.M. White, “Optofluidic microsystems for chemical and biological analysis,” Nature Photonics, vol. 5, pp. 591-597, 2011.
[2] A.L. Washburn and R.C. Bailey., “Photonics-on-a-chip: recent advances in integrated waveguides as enabling detection elements for real world, lab-on-a-chip biosensing applications,” Analyst, vol. 136, pp. 227-236, 2011.
[3] C.L. Arce et al., “Silicon photonic sensors incorporated in a digital microfluidic system,” Analytical Bioanalytical Chemistry, vol. 404, pp. 2887-2894, 2012.
[4] S. Kuhn et al., “Loss-based optical trap for on-chip particle analysis,” Lab Chip, vol. 9, pp. 2212-2216, 2009.
[5] P.C. Ashok et al., “Waveguide confined Raman spectroscopy for microfluidic interrogation,” Lab Chip, vol. 11, pp. 1262-1272, 2011.
[6] F. Prieto et al., “An integrated optical interferometric nanodevice based on silicon technology for biosensor applications,” Nanotechnology, vol. 14, pp. 907-912, 2003.
[7] N. Daldosso et al., “Comaprison among various Si_3N_4 waveguide geometries grown within a CMOS fabrication pilot line,” Journal of Lightwave Technology, vol. 22, pp. 1734-1740, 2004.
[8] I. Goykhman et al., “Ultrathin silicon nitride microring resonator for bio-photonic applications at 970 nm wavelength,” Applied Physics Letters, vol. 97, pp. 081108-1-081108-3, 2010.
[9] A. Gorin et al., “Fabrication of silicon nitride waveguides for visible-light using PECVD: a study of the effect of plasma frequency on optical properties,” Optics Express, vol. 16, pp. 13509-13516, 2008.
[10] S. Romero-Garcia et al., “Silicon nitride CMOS-compatible platform for integrated photonics applications at visible wavelengths,” Optics Express, vol. 21, pp. 14036-14046, 2013.
[11] P. Bienstman et al., “Optical modeling of photonic crystals and VCSELs using eigenmode expansion and perfectly matched layers,” Optical and Quantum Electronics, vol. 33, pp. 327-341, 2001.
[12] D. Taillaert et al., “Compact efficient broadband grating coupler for silicon-on-insulator waveguides,” Optics Letters, vol. 29, pp. 2749-2751, 2004.
[13] A.Z. Subramanian et al., “Near-infrared grating couplers for silicon nitride photonic wires,” Photonics Technology Letters, vol. 24, pp. 1700-1703, 2012.
[14] G. Roelkens et al., “Grating based optical fiber interfaces for silicon-on-insulator photonic integrated circuits,” IEEE Journal of Selected Topics in Quantum Electronics, vol. 17, pp. 571-580, 2011.
[15] S. Romero-Garcia et al., “Visible wavelength silicon nitride focusing grating coupler with AlCu/TiN reflector,” Optics Letters, vol. 38, pp. 2521-2523, 2013.
[16] W.S. Zaoui et al., “Cost effective CMOS compatible grating couplers with backside metal mirror and 69% coupling efficiency,” Optics Express, vol. 20, pp. B238-B243, 2012.